The qualification of coal degradation with the aid of micro-focus computed tomography

AUTHORS:
Jacob Viljoen[1]
Quentin P. Campbell[1]
Marco le Roux[1]
Jakobus Hoffman[2]

AFFILIATIONS:
[1]School of Chemical and Minerals Engineering, North-West University, Potchefstroom, South Africa
[2]Necsa – Radiation Science, Pretoria, South Africa

CORRESPONDENCE TO:
Jacob Viljoen

EMAIL:
13037242@nwu.ac.za

POSTAL ADDRESS:
School of Chemical and Minerals Engineering, North-West University, Private Bag X6001, Potchefstroom 2522, South Africa

DATES:
Received: 21 Jan. 2014
Revised: 21 Oct. 2014
Accepted: 17 Jan. 2015

KEYWORDS:
coal microstructure; compressive breakage; impact breakage; thermal breakage; X-ray

HOW TO CITE:
Viljoen J, Campbell QP, Le Roux M, Hoffman J. The qualification of coal degradation with the aid of micro-focus computed tomography. S Afr J Sci. 2015;111(9/10), Art. #2014-0025, 10 pages. http://dx.doi.org/10.17159/sajs.2015/20140025

The production of unwanted coal fines during the handling and utilisation of coal is a serious problem in processes that rely on large or closely sized particles. Coal degradation occurs at many different steps within the beneficiation or utilisation processes and through many different mechanisms, none of which are understood thoroughly. In an effort to describe the degradation mechanisms, the changes within a number of coal particles were tracked using micro-focus X-ray computed tomography (μ-CT). The observed changes were caused by impact loading, compressive loading and thermal shock. The resolution of the μ-CT tomograms enabled the identification and tracking of changes in the coal microstructure. A comparison of the tomograms taken before, during and after breakage and fracture showed that the microstructure of coal had an influence on the breakage characteristics. For impact- and compressive loading as well as during thermal treatment, the biggest structural contributor was shown to be the network of pre-existing cracks and cleats within a particle. Lower density macerals contributed more to breakage than the higher density macerals and any structure (pre-existing cracks, lithotypes boundaries and mineral boundaries) present within the particles had the potential to either act as a crack initiation site, change the direction of a propagating crack or arrest crack propagation. The direction of the applied loads during compressive- and impact loading was the biggest contributor to the directionality of newly formed cracks. For thermal treatment, the vitrinite rich microlithotypes showed more new crack formation compared to the other microlithotypes present. The particles also showed no evidence of devolatilisation (an increase in the porosity of the particle) but did show evidence of thermal drying (new cracks formed perpendicular to existing cracks).

Introduction

One of the biggest challenges in coal beneficiation as well as in coal utilisation is the unwanted production of coal fines, known as degradation.[1,2] The presence of coal fines in processes that rely on a closely sized feed can reduce the process efficiency.[3,4] The presence of fines in a beneficiated product can also have financial implications for the suppliers as many contracts specify penalties for product that does not meet specifications.[1,2,5-7] Fine coal is also hard to clean, relying on wet processes like flotation, spirals and dense medium cyclones to wash the coal.[5,8,9] The wet, fine coal is then significantly harder to dewater,[9-11] and due to the increased moisture content, the transport cost of fine coal is greatly increased.[8,9] The high moisture content can also incur financial penalties for out-of-spec product.[8,11]

Fines generation can occur at any step during the beneficiation process where the coal is mechanically stressed[2,6-8,12,13]: during comminution, screening, conveying, loading, stockpiling and reclaiming.[2,7,11] Fines are also generated when coal particles enter a reactor (be it a pyrolysis or combustion process) due to thermal shock and devolatilisation.[3,14-17] The presence of fines in a large particle reactor can reduce bed permeability[3,13,14,16], process efficiency[15,17-19] and throughput[13,18].

In both the case of physical degradation and thermal fracture, the breakage- and fracture-mechanisms are not well understood.[20,21] Clarification of these mechanisms can help to reduce the production of fines as well as aid the design of better comminution machines.[20,22,23] Over the years, various studies have tried to shed some light on the effect that physical properties have on the breakage characteristics of coal.[1,3,4,7,8,22-25] The effect of comminution machine properties on the breakage characteristics of coal has also been studied.[2,6,7,13,22,24,25]

For the impact breakage of coal it has been found that the drop height (impact energy) increases coal degradation.[6,7,13,22,24,25] The impact surface also influences the degradation – the harder the surface the higher the degradation.[2,6,7] The shape and orientation of the impacted particle has an influence on the breakage of coal[8,22]: rounded particles show less degradation than slab-like particles (particles where one of the three orthogonal dimensions is significantly smaller than the other two). The composition of the coal also plays a role. With an increased amount of vitrinite an increase in degradation will occur.[25] For single particles, bigger particles have lower specific breakage strengths and produce more degradation products.[1,7,22,23,25,26] This is due to bigger particles having more inherent weaknesses, and is referred to as the particle size effect.[4,23,25-27] For samples containing multiple particles and subjected to multiple drops, the removal of fines after each drop increased the total fines generation when compared to the same amount of drops without removal of the fines. This is referred to as cushioning.[2,6,13]

The size effect is also documented for the compressive loading of coal.[27] During uniaxial strength tests, coal samples undergo a reduction in strength as the sample size increases, until a characteristic value is reached in samples with a diameter larger than 1.5 m.[27] This is again due to an increased amount of defects present in the larger samples.[21,27] These defects include micro-cracks, cleats and inclusions. Fatigue is another mechanism that has an effect on the compressive breakage strength of coal.[7,21,23] Fatigue is the repeated application of a force, which although not strong enough to damage a particle, eventually destroys the particle due to damage accumulation within the particle.

For thermal fracture, it was found that an increase in furnace temperature causes the degradation to increase.[17,28] An increase in particle size increases both the size of the progeny as well as the particle count of the progeny.[17,19,28] In addition, the longer the particle stayed in the furnace, the lower the particle count became due to the progeny being burnt away.[17,28] It was also found that an increase in the volatile content of the particles increased the degradation,[15,19] although some authors found no connection between volatile content and fragmentation.[28] Taking this into account, Dacombe et al.[28] postulated that there are two mechanisms responsible for thermal degradation: exfoliation and fragmentation. Exfoliation is the formation of many small progeny from the outside of the particle[15,28] and occurs due to thermal stresses that occur at higher heating rates.[15,17,28] Fragmentation is when the particle centre remaining after exfoliation breaks into larger (when compared to exfoliation) progeny and happens due to the build-up of internal pressure as the volatile matter in the coal particle is released.[15,17,28]

A common theme in all of the degradation scenarios is the presence of micro-defects within the particles. These micro-defects can act as sites where crack propagation can either start or arrest.[29] Micro defects that can occur within coal are mineral inclusions[23,25], pre-existing cracks and cleats[23,25,27,30,31] as well as microlithotype boundaries[23,25]. The macerals that occur in coal can be grouped into three main classes: vitrinite, inertinite and liptinite.[32,33] For coal degradation, vitrinite is the most important one, as it is known to be a very brittle, weak maceral.[25,27] It also has the most flaws present[25,27], as it experiences the highest degree of shrinkage during coalification[32]. Cleats are cracks that are inherent to coal and are formed during the coalification process by the shrinkage and expansion of the coal matrix.[27,30,32,34] The mineral inclusions present in coal are usually in the form of either discrete mineral inclusions[35] or cleat filling minerals[32,35]. The minerals can become part of the coal matrix through detrital deposition[35] and through biogenic-, syngenetic- or epigenetic precipitation.[32,35] Various studies have applied micro-focus X-ray computed tomography to identify these microstructures in coal.[36-42]

X-ray computed tomography (μ-CT) is a technique that was originally developed in the medical sciences where it is commonly used during diagnostic radiology.[31,36,37,43] Since the 1980s, the technique has also been widely used in the geosciences for non-destructive characterisation.[31,36,37,39,43] During the application of the technique, an X-ray cone beam is projected at and through the sample to be analysed. As the beam travels through the sample, the intensity of the beam diminishes due to absorption and scatter from the direct beam path. A detector records the intensity of the beam after it passes through the sample as a radiograph.[30,33,43-45] A number of radiographs, made by rotating the sample along its axis, is combined to form a tomogram, or a three-dimensional representation of the scanned sample, using filtered backprojection.[33,36,40,41,43,44] A detailed mathematical treatment of the technique and reconstruction is beyond the scope of this study. There is however a large body of literature available on the subject.[33,36,38,39,43,46]

The attenuation coefficient or tomo-density determines the absorption and scattering of the X-ray energy from the direct beam path and is a combination of the physical density, mean atomic number of the sample elements and the energy of the X-ray beam.[38,39,45]

Micro-focus X-ray computed tomography (μ-CT) is an improvement over traditional medical CT. These improvements are mostly because there is no limit to the radiation dose that can be applied to samples typically scanned using μ-CT.[36] Higher energies, longer exposure times and higher resolutions are therefore possible.[36] The resolution of a medical CT is in the range of 250 X 250 X 250 μm[39] to 0.6 X 0.6 X 1 mm[16,31,37], while the resolution of a μ-CT tomogram can be as low as 10 X 10 X 10 μm[31,33,37,46], depending on the size of the sample that is to be analysed[45,46]. This reduction in resolution is due to the minimisation of the X-ray spot size by focusing the electron beam prior to hitting the target[39,45] as well as by lowering the X-ray current[39,43]. The focussing of the electron beam also has another advantage, namely the reduction of the geometrical unsharpness.[45]

The aim of this study is to explore the applicability of μ-CT as an analytical tool in the study of coal breakage and degradation, and forms part of a larger study on coal degradation. To this end, a small number of samples were loaded, mechanically and thermally, and μ-CT was used to track the breakage that took place during loading. Changes to the experimental set-ups that may improve the experimental accuracy were also recommended.

Experimental methods

All of the tomograms for the experiments below were generated on the Nikon XTH 225 ST system, manufactured in England and housed at the South African Nuclear Energy Corporation (Necsa) in their Micro-focus X-ray Radiography and Tomography (MIXRAD) department. The system is operational between 30 kV and 225 kV, and between 0 mA and 1 mA with a point source of between 1 μm and 3 μm. The detector is a 400 X 400 mm flat Perkin Elmer panel detector with 200 X 200 μm pixels. All tomograms were generated with 1000 projections in 360º and an exposure time of 1 s per projection. The resolutions obtained during these studies varied from 17 μm to 50 μm depending on the size of the samples. Hoffman and De Beer[40] give a detailed description of the MIXRAD facility. All of the reconstructions were performed using Metris CT-Pro and the analyses were done using the VGStudio Max 2.1 visualisation software package.

All of the mechanically loaded particles were wrapped in GLAD® cling film to minimise the loss of material during breakage and to simplify the comparison of the before and after tomograms. It is assumed that the radio translucent cling film did not deteriorate the quality of the tomograms, as the cling film has a low physical density (0.92 g/cm^3)[47] and the sample was wrapped in a very thin layer of the film.

The experimental procedures for all three types of degradation experiments (compression loading, impact loading and thermal treatment) are given below.

Compressive loading

To determine the effect of the internal structures on the compression breakage characteristics, two experiments were conducted. During the first experiment, the samples were prepared from a single large (approximately 1 x 0.5 x 0.4 m) block of run of mine (ROM) coal sourced from the Waterberg coalfield in South Africa. The samples, prepared from the heterogeneous, bright-dull banded lithotypes, were cut into 30 X 30 X 30 mm square particles. Two surfaces, on opposite sides of the particle, were machined flat and uniaxial compression was applied to these surfaces. Six samples were sent for data acquisition at the MIXRAD facility. After data acquisition, the particles were wrapped in cling film, loaded into a Monsanto tensometer, supplied by IMP, and compressed while the displacement was measured. Figure 1 shows the Monsanto tensometer (left) that was used during the first round of compression tests and the experimental set-up used during the impact breakage tests (right). The labels on the left of Figure 1 indicate the load cell (A) that was used to measure the applied load during the compression tests and two surfaces between which the particles were compressed (B). The load was applied either perpendicular or parallel to the bedding plane until the first crack that split the parent particle into two or more progeny was detected and the force required to generate the first fatal crack (load at first fracture) was recorded. The load at first fracture was measured as the applied force where the displacement showed a sudden increase. After loading, the particles were again scanned and the tomograms generated before and after fracture compared. From the comparison, new crack formation, probable crack initiation sites and propagation routes were identified. The tomograms were generated at 100 kV and 100 μA and an average spatial resolution of 24 μm was achieved.

During the first set of experiments, it was found that it is very hard to come to a solid conclusion as to the probable propagation routes of the cracks if the only information available is at the start and at the end of the loading cycle. A second set of experiments were undertaken in which two additional samples were subjected to compressive loading that was incrementally increased. The particles were placed into a specifically designed, radio translucent test cartridge manufactured (at the North-West University) from poly(methyl methacrylate) in such a fashion that

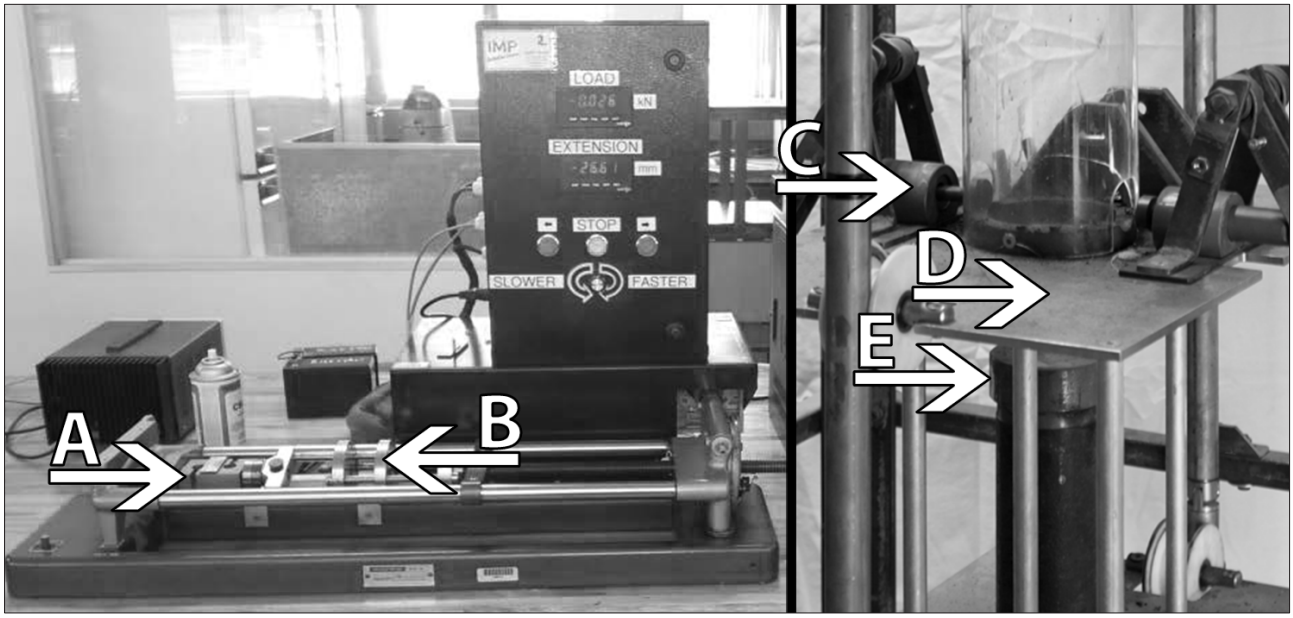

A, load cell; B, the compression surfaces of the tensometer; C, sample clamps; D, impact carriage; E, impact anvil.

Figure 1: Experimental set-ups for the compressive breakage tests (left) and the impact breakage tests (right).

the uniaxial compressive force applied to the particle could be increased incrementally. The particle placed in the cartridge was scanned, the applied load increased and the particle scanned again. This process of tomogram generation and load increase was repeated until the particle failed. All of the tomograms generated were compared to determine new crack formation, crack initiation sites and crack propagation routes. Tomograms were generated at 130 kV and 100 μA with a spatial resolution of 29 μm.

Impact loading

A number of coal particles were prepared from a single block of ROM coal sourced from the Waterberg coalfield. The samples were cut to 50 X 50 X 50 mm square particles and three sides machined flat – one side where the impact was to take place and two sides, opposite one another, where the sample clamps gripped the particles. In order to ensure that there were as many maceral boundaries and pre-existing cracks as possible to study, the samples were prepared from the bright-dull banded lithotypes of the block and impacted parallel and perpendicular to the bedding planes. The crack network for each particle was characterised using μ-CT, wrapped in cling film and dropped onto a steel anvil at 4.5 m/s. The impact velocity is equivalent to a drop from 1 m. The rig was developed at the North-West University and manufactured in such a way that the bedding plane orientations of the particles could be accurately controlled. Half the particles were dropped with the bedding planes parallel to the impact surface and the other half with the bedding planes perpendicular to the impact surface. After the particles were dropped, they were again scanned using μ-CT. Figure 1 shows the Monsanto tensometer (left) that was used during the first round of compression tests and the experimental set-up used during the impact breakage tests (right). The labels on the right side of Figure 1 indicate the sample clamps (C), impact carriage (D) and impact anvil (E). The tomograms generated both before impact and after were generated at 160 kV and 70 μA and an average spatial resolution of 48 μm was achieved. A comparison of the before and after tomograms were made and new crack formation, crack initiation sites and probable propagation routes were identified.

Fracture from thermal treatment

In order to determine the effect of maceral boundaries and crack network on the thermal breakage properties of coal, a number of cylindrical samples, with a height of 30 mm and a diameter of 19 mm, were prepared from large particles of a Witbank coal. Witbank coal was used to prevent any damage to the graphite crucibles as the Witbank coal is non-swelling while the Waterberg coal is a medium-swelling coal. The prepared samples were placed in graphite crucibles that could be rapidly heated in a radio frequency induction furnace built by Necsa. The mechanical sample preparation was undertaken to ensure that the samples fitted tightly into the radio translucent graphite crucibles. This was to ensure that a clear tomogram was generated. If the samples did not tightly fit in the crucibles, there would be the possibility of the samples moving while being scanned, introducing errors and reducing the sharpness of the tomogram. The crucibles containing the samples were scanned before and after being heated and comparisons of the tomograms made to determine new crack formation, crack initiation sites and probable crack propagation routes. The heating rate within the graphite crucible was controlled by changing the potential difference through the radio frequency furnace coil and the maximum temperature controlled by the residence time within the furnace. The heating rates ranged from 27 ^{o}C/s to 76 ^{o}C/s with final temperatures reaching between 700 ^{o}C and 800 ^{o}C. The residence times varied between 9 s and 29 s. The heating rates, maximum temperatures and residence times were varied for all samples. All experimental runs were conducted in an air atmosphere. The temperatures stated are the outside crucible temperatures, and were measured using a pyrometer that determines the crucible temperature by the infrared radiation it emits. Owing to the exploratory nature of the study and the difficulty of measuring the internal temperature without introducing errors, the internal temperatures were not measured or estimated. The particle temperature was, however, high enough to cause thermal drying but not so high as to cause any detectable devolatilisation. The tomograms were generated at 130 kV and 100 μA with voxel sizes of 17 μm. A comparison to determine new crack formation, crack initiation sites and probable propagation routes was made.

Results and discussion

Figures 2 to 9 show comparisons of slices from the tomograms generated. The slices on the left in all figures are from the tomograms generated before loading (or thermal treatment) while the slices on the right are from the tomograms generated after loading. Where there are three slices in a figure, the centre slice is from a tomogram generated during loading.

In all of the tomogram slices presented in this study, the varying shades of grey represent the variation in the linear attenuation of the particles. Black areas are areas where no sample material is present; dark grey areas are areas of lower attenuation; light grey areas are areas of higher attenuation and white areas represent mineral matter. The light grey macerals are assumed to be either inertinite- or carbominerite-rich microlithotypes, while the darker grey areas are assumed to be vitrinite rich microlithotypes. This is due to the higher density of the inertinite- and carbominerite-rich macerals compared to the vitrinite rich macerals.[48,49]

Compressive loading

Figure 2 shows a comparison of the before and after tomogram of a particle that was compressed perpendicular to the bedding plane in the Monsanto tensometer, while Figure 3 shows a particle loaded parallel to the bedding plane. The load application perpendicular to the bedding plane indicates that the particle was compressed from the top and bottom of the slice given in Figure 2, while the parallel load application indicates that the particle in Figure 3 was compressed from the left and right of the slice.

Both particles shown were prepared from the bright-dull banded lithotype of a single block of ROM coal from the Waterberg coalfield. All the arrows marked (F) in both Figure 2 and 3 show cleats or cracks that existed in the pre-loaded particles that enlarged during compression. The arrows marked (M) show mineral inclusions that may have had an influence on either crack initiation or crack propagation. Lastly, arrows marked (P) show either maceral-maceral boundaries or maceral-mineral boundaries that may have had an influence on crack initiation or propagation.

Figure 2 shows a number of cracks present in the original crack network that enlarged during compression. The largest new crack formed during compression, however, is the crack that runs down the middle of Figure 2 (through M), in the post compression slice (right-hand slice). This newly formed fracture did not form from any crack present and, although it did propagate through the mineral inclusions at M, shows no influence of any microstructure in the particle. It is speculated that the newly formed crack is due to load concentration where the tensometer contacted the particle, thus forming a crack in the direction of the applied load. Because of the manual sample preparation, the sides of the particle could not be made perfectly smooth and parallel. This created some features where stress concentration could take place.

In Figure 3 it can again be seen that the major, newly formed cracks (through P_1; M_1 and M_2) formed parallel to the applied load, i.e. from the left and right. The left-hand slice shows a significant number of cracks (marked F) that contributed to the new crack network; the majority of the cracks that are perpendicular to the load direction are due to the enlargement of these pre-existing cracks. P_1 shows where more new cracks formed in the vitrinite rich microlithotypes compared to the inertinite rich microlithotypes. P_2 shows where a boundary between two macerals caused the propagating crack to change direction. M_1 shows a probable crack initiation site at a mineral inclusion, while M_2 shows a mineral inclusion that was in the path of a propagating crack. This inclusion may have helped with the crack propagation.

From the comparisons above, it seems that the direction of the applied load has a great influence, with the majority of the newly formed cracks propagating in the direction of load application. The cracks that did not form in the same direction as the load application are due to pre-existing cracks. In addition, of the microstructures present, the existing crack or cleat network has the greatest influence on crack initiation and propagation, with very few of the pre-existing cracks showing no change. It is also clear that the lower density macerals show more new crack formation than the higher density macerals and in some cases, the boundaries between two macerals influenced the crack propagation.

Although it is possible to speculate which of the microstructures influenced the propagation and the chronology of the newly formed cracks, it is impossible to say so with certainty. To clarify this, another set of experiments was performed where the load application to the samples was increased incrementally until the particle failed, with the internal structure of the sample investigated after every increase. This was done to try to determine, with a higher degree of certainty, which of the microstructures would have a higher probability of influencing the crack propagation. To this end Figure 4 and Figure 5 show three steps in the compression process of two particles that were compressed perpendicular (Figure 4, loaded top to bottom) and parallel (Figure 5, loaded top to bottom) to the bedding planes. Although there were many tomograms generated during the incremental load increase, Figures 4

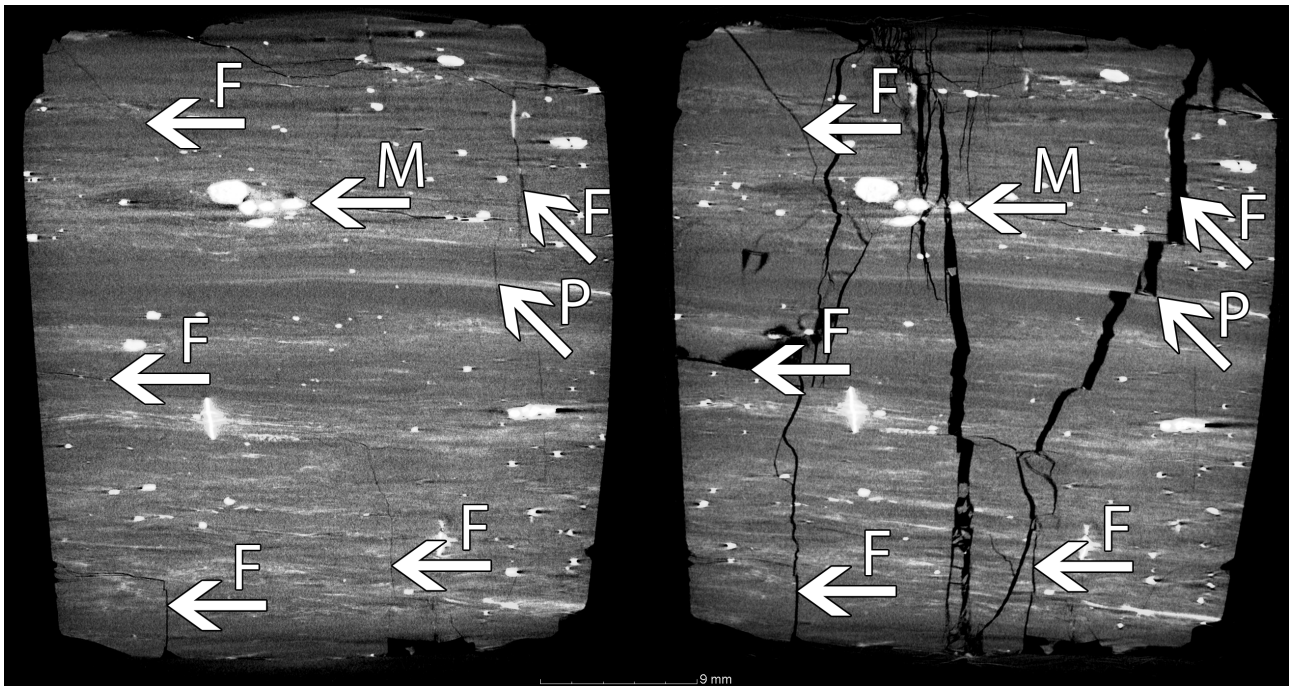

F indicates cleats or cracks that existed in the pre-loaded particles that enlarged during compression; M indicates mineral inclusions that may have had an influence on either crack initiation or crack propagation; P indicates either maceral–maceral boundaries or maceral–mineral boundaries that may have had an influence on crack initiation.

Figure 2: Comparison of the before (left) and after (right) tomogram of a particle compressed perpendicular to the bedding plane in the Monsanto tensometer.

and 5 show only the tomograms generated before loading, after loading and a single tomogram generated during compression. The samples were again prepared from the bright-dull banded lithotypes of the large block of Waterberg ROM coal. The arrows marked F, M and P have the same meaning as in Figures 2 and 3.

The labels marked F_1 in Figure 4 show a number of cracks that are thought to contribute to the formation in the large crack in the far right slice of Figure 4. The label P shows a maceral-maceral boundary that influenced the crack propagation while M shows a mineral inclusion that did the same. F_2 shows a number of cracks that were present in the particle, but due to the pressure applied, closed in the middle slice. Another crack that closed while being compressed is shown at F_3. Even though the closed crack is no longer apparent in the middle slice, this does not mean that the closed crack no longer contributes to crack propagation. In the final slice it is clear that the closed crack influenced the propagation of the crack through F_1 and F_3.

Figure 5 again shows some pre-existing cracks (F) that contributed to the final crack network, as well as a lower density maceral (P_1) where a higher amount of newly formed cracks can be observed. P_2 shows a maceral-maceral boundary that also contributed to the propagation of a crack. Figure 5 shows no cracks that closed due to the applied load, in fact, the opposite is observed: there are some cracks that, despite the load applied perpendicular to the cracks, enlarged.

From the incremental loading, the same conclusions can be reached regarding the effect of the directionality of the applied load, as well as to the influence of the original microstructure on the crack evolution. It was also observed that in the particle where the compression was

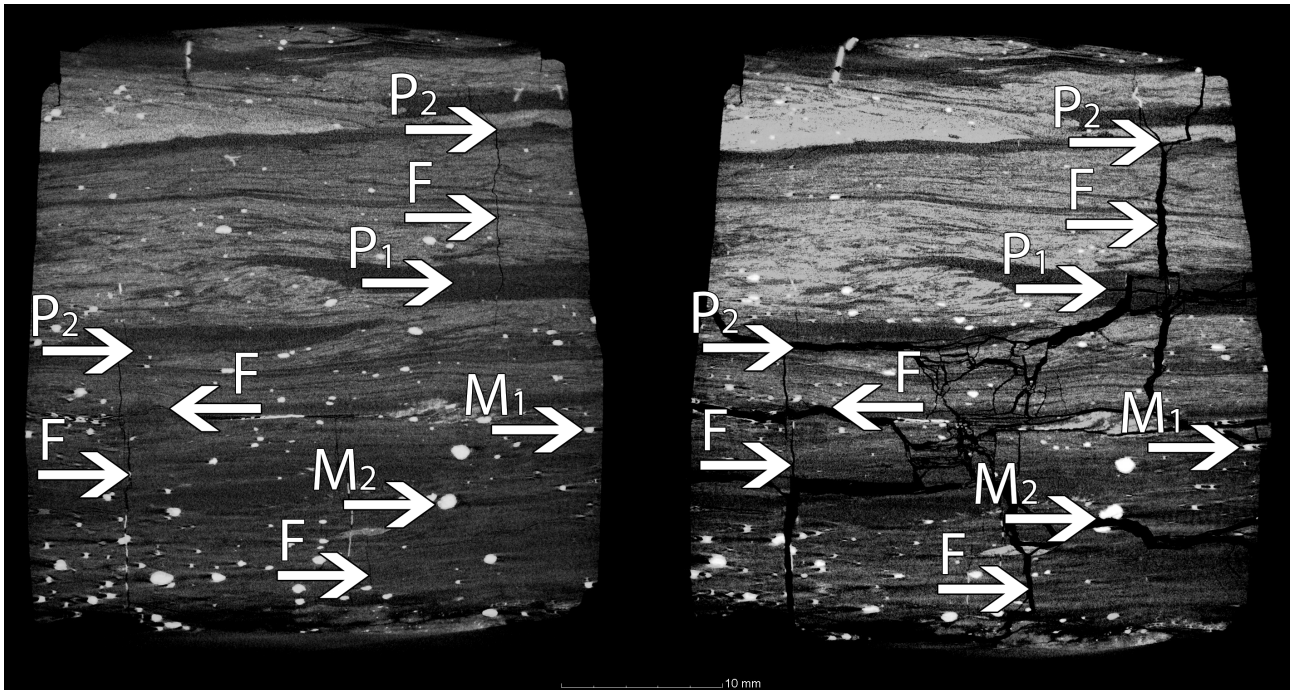

F indicates cleats or cracks that existed in the pre-loaded particles that enlarged during compression; M indicates mineral inclusions that may have had an influence on either crack initiation or crack propagation; P indicates either maceral–maceral boundaries or maceral–mineral boundaries that may have had an influence on crack initiation.

Figure 3: Comparison of the before (left) and after (right) tomogram of a particle compressed parallel to the bedding plane in the Monsanto tensometer.

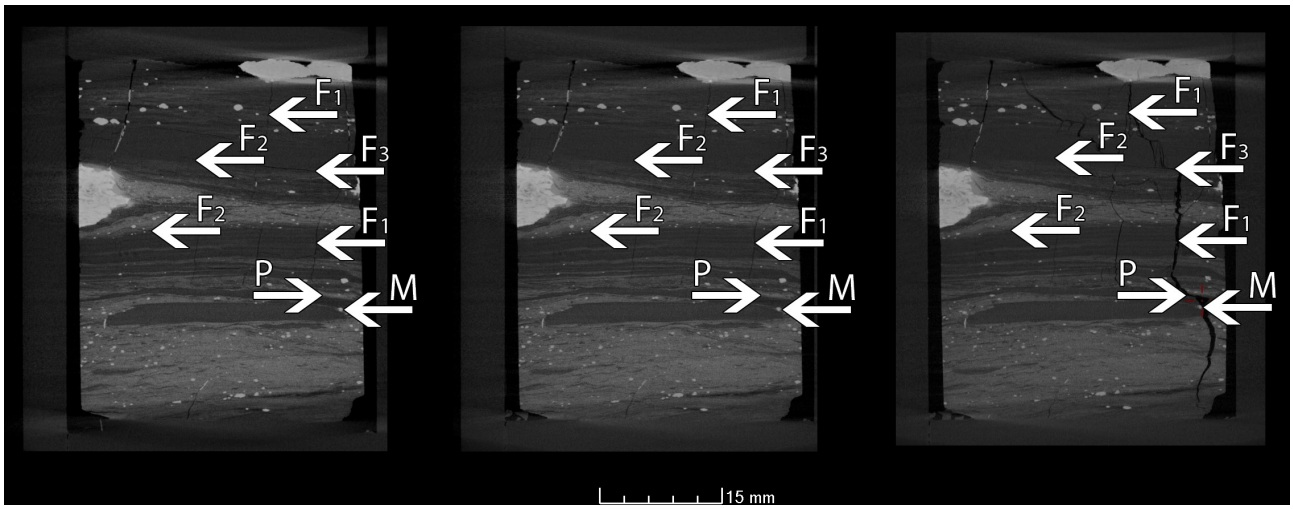

F indicates cleats or cracks that existed in the pre-loaded particles that enlarged during compression; M indicates mineral inclusions that may have had an influence on either crack initiation or crack propagation; P indicates either maceral–maceral boundaries or maceral–mineral boundaries that may have had an influence on crack initiation.

Figure 4: Comparison of a particle before (left) and after (right) compression incrementally perpendicular to the bedding plane.

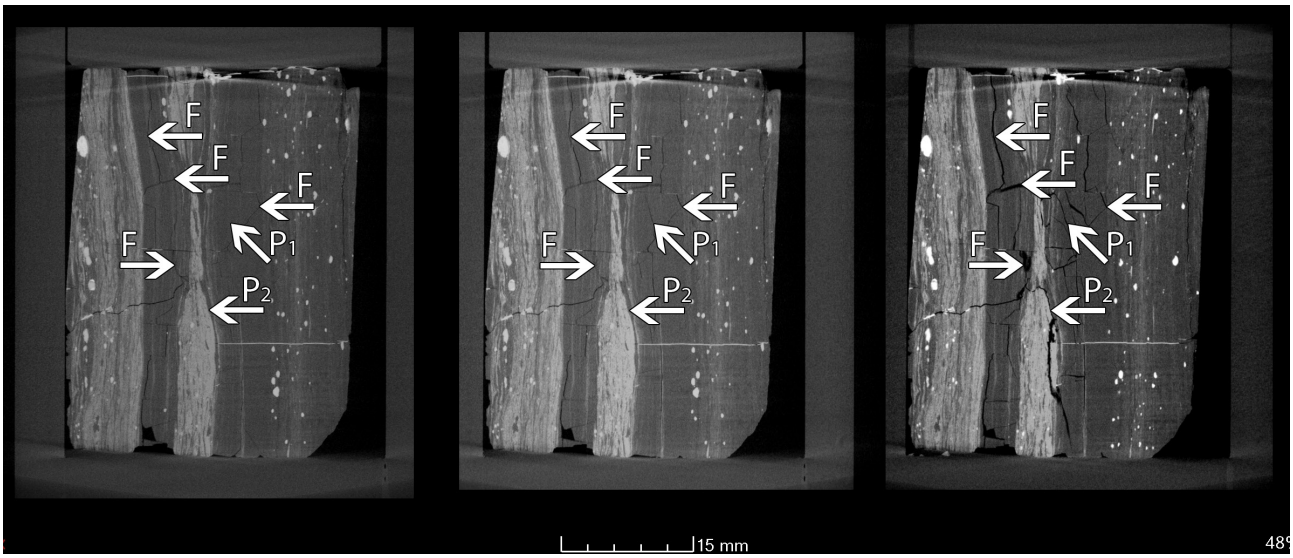

F indicates cleats or cracks that existed in the pre-loaded particles that enlarged during compression; P indicates either maceral–maceral boundaries or maceral–mineral boundaries that may have had an influence on crack initiation.

Figure 5: Comparison of a particle before (left) and after (right) compression incrementally parallel to the bedding plane.

perpendicular to the bedding plane, some of the cracks that were perpendicular to the applied load closed due to the applied load. This was only observed in the particle that was compressed perpendicular to the bedding plane.

From the comparison it is clear that the incremental load increase is still too large to deduce with any higher degree of certainty the propagation routes and hierarchy. Owing to the time required to generate a tomogram, the crack propagation cannot be observed, only the after effects i.e. the newly formed cracks. If the load increase with each increment is reduced and more tomograms generated during compression (6–8 tomograms generated instead of 3–4), it may be possible to observe the order in which new cracks form and the propagation routes deduced.

Impact loading

Figures 6 and 7 show comparisons of the tomograms generated before and after impact of two samples prepared from a large block of ROM coal sourced from the Waterberg coalfield. The samples in both Figure 6 and Figure 7 were impacted onto a steel anvil at a velocity of 4.5 m/s. The impact velocity was equivalent to a drop from 1 m, a low impact velocity selected specifically to study the degradation at low impact energy. Figure 6 shows a particle that was impacted with the bedding plane parallel to the anvil while Figure 7 shows a particle that was impacted with the bedding plane perpendicular to the anvil. In both Figure 6 and Figure 7, the surface of the particle that was in contact with the impact anvil (impacted surface) is the bottom edge of the slice or the edge closest to the scale bar.

In Figure 6, the majority of the cracks that formed, formed from pre-existing cracks (F) within the particle. There were however some new cracks that formed in the lower density, vitrinite rich, macerals (P).

Figure 7 also shows a number of existing cracks that enlarged during impact. Some of the other trends observed in the compression loaded particles can also be seen in Figure 7. Here P_1 shows where a newly formed crack propagated along a maceral boundary and P_2 indicates cracks formed in a vitrinite rich microlithotype. Several cracks end at the mineral inclusion indicated by M in Figure 7.

From the comparisons made in both Figure 6 and Figure 7, it is clear that the main contribution to crack initiation and propagation is the existing crack network of the coal. The final crack network did not show a high dependence on the direction of the applied impact load when compared to the compressive loading in Figures 2 to 5. It is hypothesised that this is due to the low impact velocity, equivalent to a drop of approximately 1 m onto a steel plate. This is supported by various studies where it was found that that a higher drop height increased the breakage and degradation.[6,7,13,22,24,25]

Fracture from temperature increase

Figures 8 and 9 show comparisons of the tomograms generated before and after thermal treatment. A Witbank coal was used rather than a Waterberg coal to prevent damage to the graphite crucibles. Figure 8 shows the comparison of a particle heated to 800 °C at a rate of 31 °C/s. Figure 9 shows the comparison of a particle heated to 700 °C at a rate of 51 °C/s.

Figure 8 shows two fractures (F) present in the coal before heating, both of which contributed to crack propagation. The crack that propagated along the line indicated by the arrows marked M shows the crack did not propagate through the mineral inclusions but along the outside of the tiny mineral inclusions. It is assumed that the two cracks that formed from the initial cracks marked F were the first to form. Note that many of the cracks that radiate from these initially formed cracks do so almost perpendicular to the main cracks. According to Mathews et al.[50], this occurs during thermal drying due to particle shrinkage. Figure 8 also shows no structural changes indicative of devolatilisation, indicating a discrepancy between the outside crucible temperature and the particle temperature.

Figure 9 shows that during the thermal treatment of coal, pre-existing cracks (F1) present in coal enlarge. Again it can be seen in Figure 9 that new cracks form perpendicular to pre-existing cracks (F2) indicating that thermal drying took place. The enlarged sections in Figure 9 show that the vitrinite rich layers, indicated by P, show an increase in new crack formation when compared to the rest of the particle. The enlargements in Figure 9 also show how the vertical, mineral filled cleats act as discontinuities, with cracks terminating at the mineral filled cleats.

In both Figures 8 and 9, it was observed that pre-existing cracks expanded during the thermal treatment of coal particles. It is also assumed that any new cracks that form will do so either from an initial crack or in the lower density macerals, and crack propagation will occur along lines of weakness such as maceral-mineral boundaries.

Even though the heating rates (27 °C/s, 51 °C/s, 31 °C/s and 76 °C/s), final temperatures (700 °C, 750 °C and 800 °C) and residence times (9 s, 13 s 25 s and 29 s) were varied, no influence of these changes

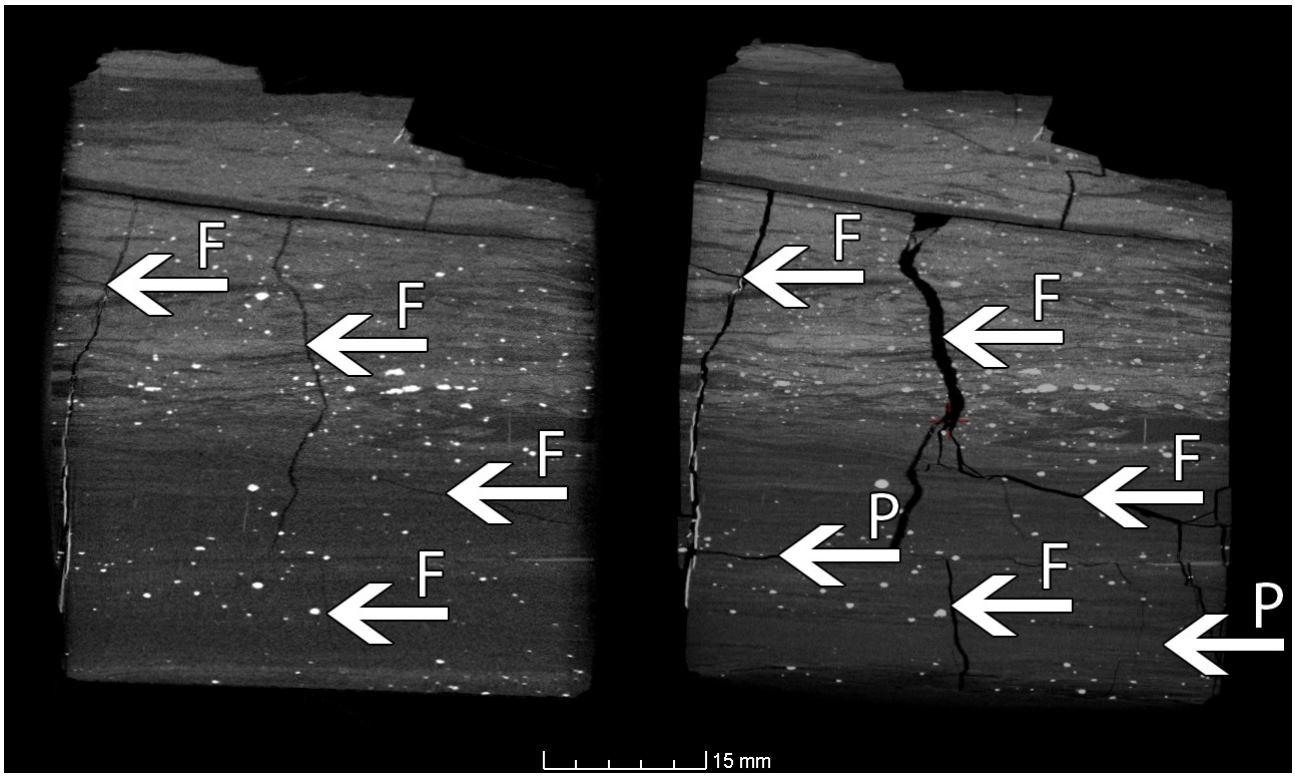

F indicates cleats or cracks that existed in the pre-loaded particles that enlarged during compression; P indicates either maceral–maceral boundaries or maceral–mineral boundaries that may have had an influence on crack initiation.

Figure 6: Comparison of a particle before (left) and after (right) impaction with the bedding plane parallel to the anvil.

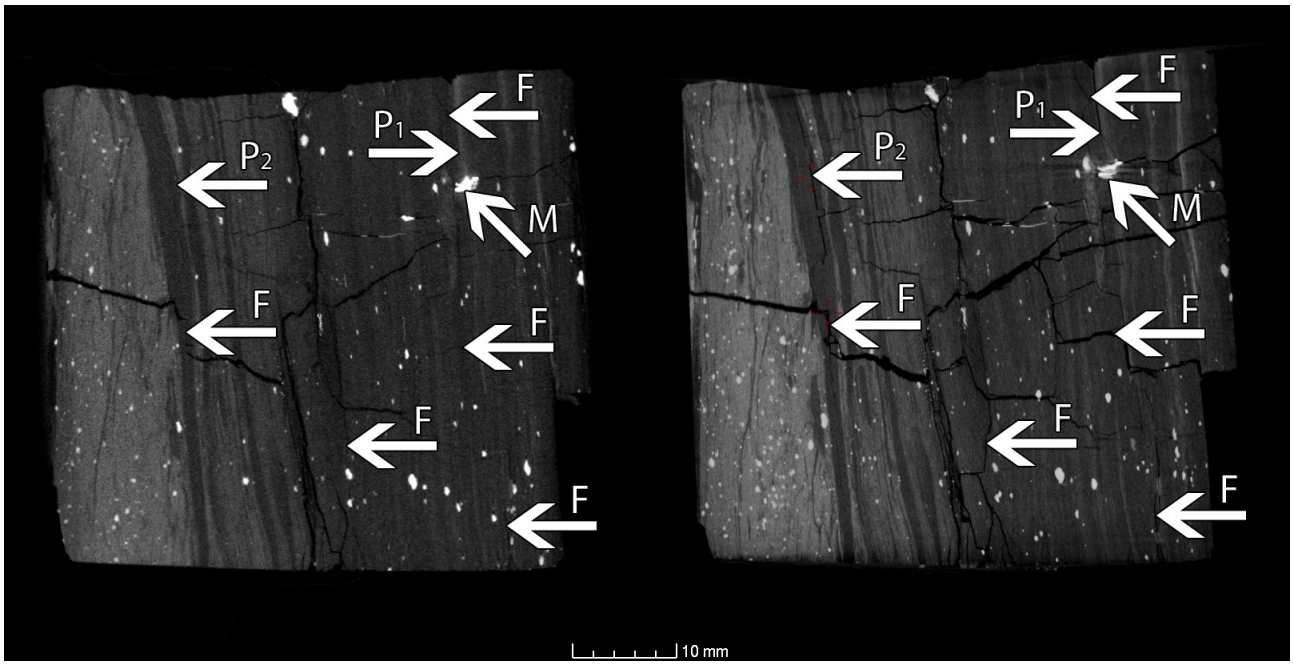

F indicates cleats or cracks that existed in the pre-loaded particles that enlarged during compression; P indicates either maceral–maceral boundaries or maceral–mineral boundaries that may have had an influence on crack initiation.

Figure 7: Comparison of a particle before (left) and after (right) impaction with the bedding plane perpendicular to the anvil.

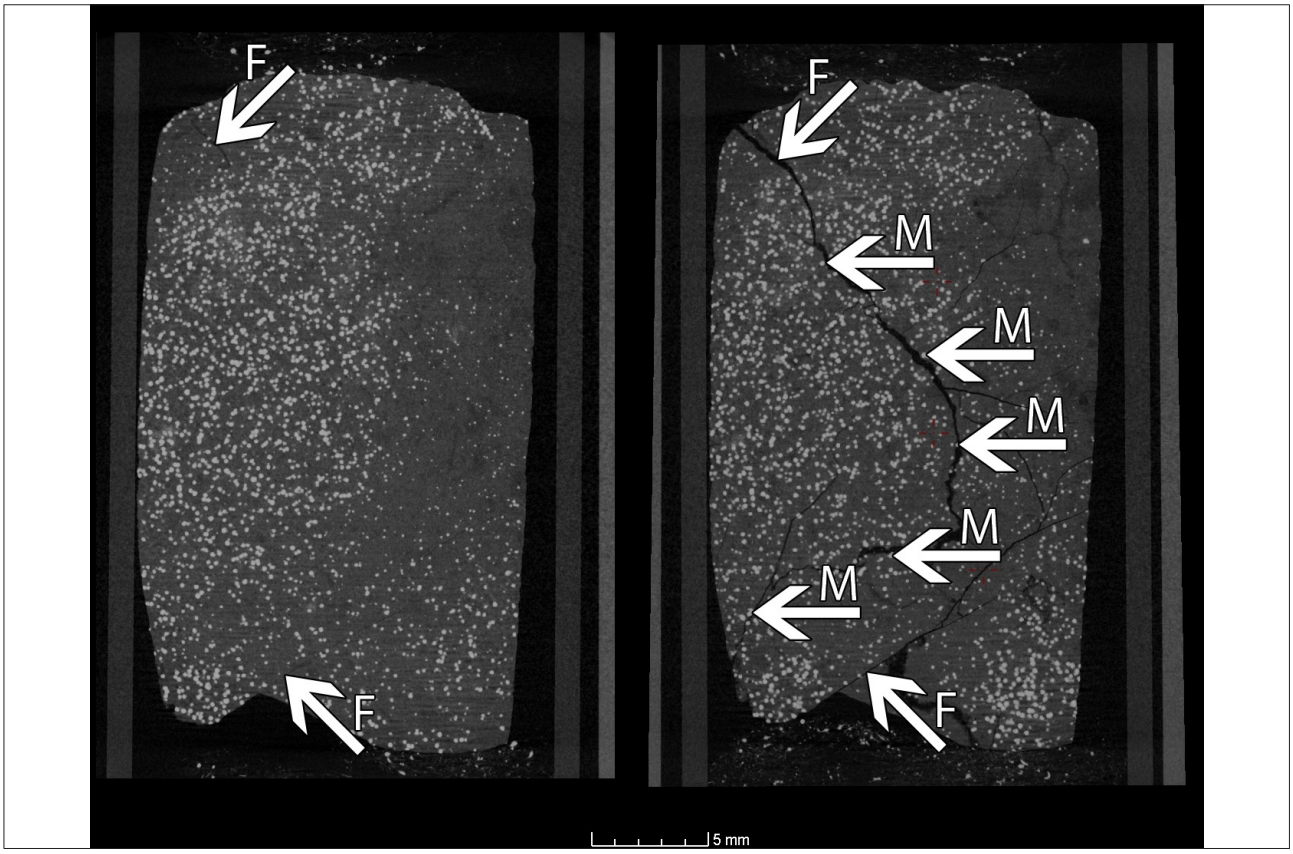

F indicates cleats or cracks that existed in the pre-loaded particles that enlarged during compression; M indicates mineral inclusions that may have had an influence on either crack initiation or crack propagation.

Figure 8: Comparison of a particle before (left) and after (right) it was heated to 800 ºC at a rate of 31 ºC/s.

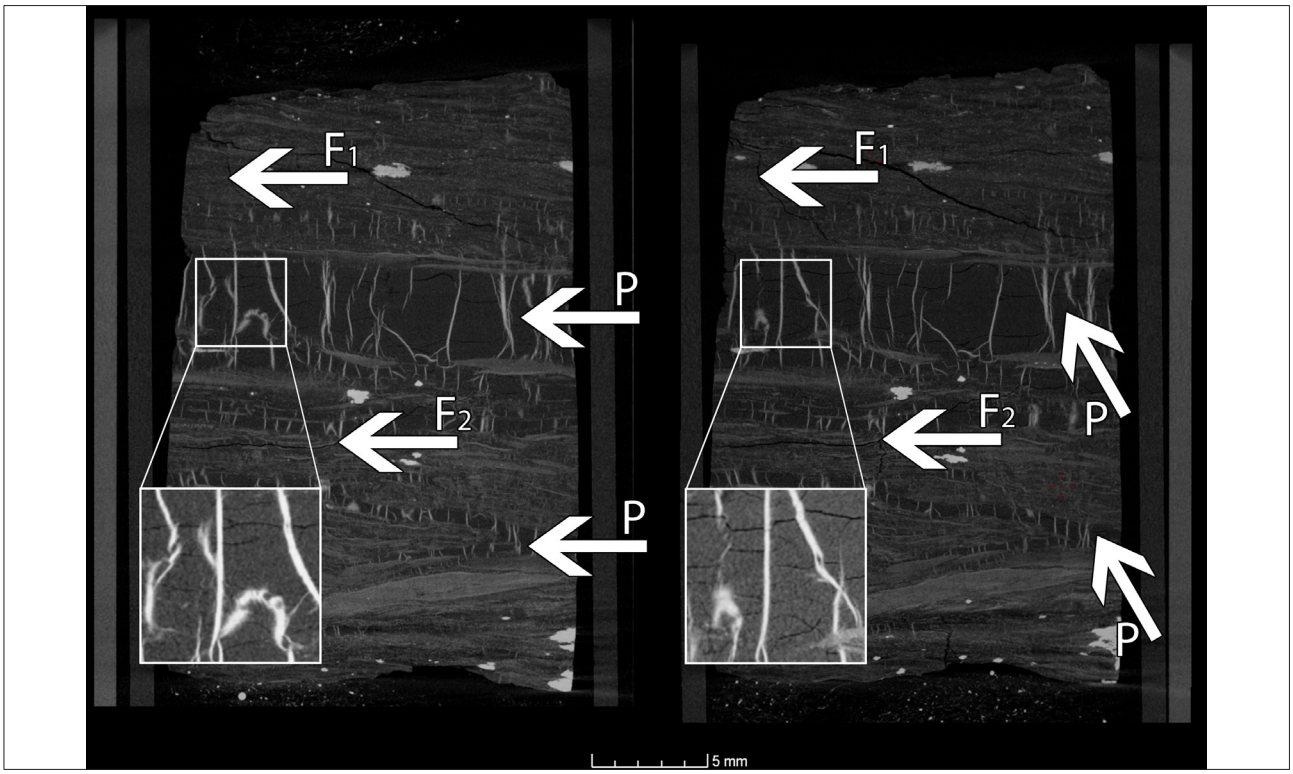

F indicates cleats or cracks that existed in the pre-loaded particles that enlarged during compression; P indicates either maceral–maceral boundaries or maceral–mineral boundaries that may have had an influence on crack initiation.

Figure 9: Comparison of a particle before (left) and after (right) it was heated to 700 ºC at a rate of 51 ºC/s.

could be detected. It is assumed that this is due to the residence times being far too short for the particle temperature to reach the maximum crucible temperature. Although there is no evidence of devolatilisation taking place, the particle did show evidence of thermal drying.

Conclusion

The microstructure of coal was investigated using μ-CT to determine if the influence of the microstructure on the coal breakage characteristics can be ascertained. To this end, a number of degradation processes were simulated using single particles: slow compression breakage, impact breakage and primary (thermal) fracture. During the mechanical loading, a number of particles were prepared from a ROM sample of Waterberg coal and loaded in such a way that the influence of the microstructures could be identified. The following conclusions were drawn from the comparisons:

- During the compressive loading of coal, one of the biggest influences on the enlargement of existing cracks and the propagation of newly formed cracks is the direction of the applied load.
- It was found that if a particle is compressed with the bedding plane perpendicular to the load direction, some of the cracks along the bedding plane will close. The cracks that do close will still influence the development of the crack network around them, as other cracks can still terminate and initiate within them. This was not observed with the particles loaded parallel to the bedding plane.
- In both the compressive and impact loading scenarios, the pre-existing cracks within a particle have the biggest influence of the microstructures present.
- The macerals and maceral boundaries also influence the formation of new cracks and the crack propagation; the lower density, vitrinite rich, macerals showing a tendency towards increased crack formation and some of the maceral boundaries can affect the propagation of a crack.

For the thermal loading of coal, samples were hand selected and prepared from a large sample of washed and sized Witbank coal and exposed to various temperatures and heating rates. The conclusions drawn are as follows:

- The pre-existing crack network influences the final network by increasing both in length and aperture; the network also acts as an initiation site for new cracks.
- The lower density macerals show a propensity to form more new cracks than do the denser macerals.
- Cracks propagate along the maceral-mineral boundaries.

Thus, it is clear that the microstructure of coal can be identified using μ-CT as an analytical technique. The change in the microstructure can also be tracked using μ-CT, but some modifications to the experimental procedures and set-ups are required to tell with greater certainty how the cracks formed and propagated. For the compressive loading of coal, the incremental load increase should be reduced to try to isolate the decisive moments in the very fast crack initiation and propagation process. For the impact loading of coal, the impact energy range should be expanded (i.e. higher impact energies and lower impact energies) to enable the study of the effect of impact energy on crack development. This will allow for a better understanding of the mechanisms by which coal breaks during impact. Finally, according to literature, temperature, heating rate and residence time affects the thermal degradation of coal but none of these effects were seen in this study. Should the ranges for the temperature, heating rate and residence times be increased, and the internal temperature gradients determined, a better understanding of crack development during heating can be gained.

Acknowledgements

We thank Juan Nelson, Wynand Breytenbach, Charlotte Badenhorst and Carla Hatting for their help with the experimental work; the personnel at the MIXRAD facility, Necsa for their assistance, patience and enthusiasm and two anonymous reviewers for their invaluable input. This project was funded by the Southern African Coal Processing Society. The work presented in this paper is based on research supported by the South African Research Chairs Initiative of the Department of Science and Technology and National Research Foundation (NRF) of South Africa (Coal Research Chair grant no. 86880). Any opinion, finding, conclusion or recommendation expressed in this material is that of the authors and the NRF does not accept any liability in this regard.

Authors' contributions

J.W.H. is a tomographic instrument expert and was responsible for the generation of the tomograms used during this study and significant editing of the manuscript. M.L.R. and Q.P.C. were the project leaders and initiators; they were also responsible for the experimental concept and significant editing of the manuscript. J.V., M.L.R. and Q.P.C. were responsible for the experimental design. J.V. was responsible for some of the experimental work, the analysis of the generated tomograms and writing the manuscript.

References

1. Teo CS, Waters AG, Nicol SK. Quantification of the breakage of lump materials during handling operations. Int J Miner Process. 1990;30(3/4):159–184. http://dx.doi.org/10.1016/0301-7516(90)90013-O
2. Sahoo RK, Roach D. Effect of different types of impact surface on coal degradation. Chem Eng Process. 2005;44(2):253–261. http://dx.doi.org/10.1016/j.cep.2004.02.019
3. Bunt JR, Waanders FB. An understanding of lump coal physical property behaviour (density and particle size effects) impacting on a commercial-scale Sasol-Lurgi FBDB gasifier. Fuel. 2008;87(13):2856–2865. http://dx.doi.org/10.1016/j.fuel.2008.03.022
4. Eswaraiah C, Gupta A, Nagarajan R, Rajavel M, Nandakumar K. Minimization of fines generation in size reduction of coals by impact crusher. Fuel Process Technol. 2008;89(7):704–714. http://dx.doi.org/10.1016/j.fuproc.2008.01.001
5. England T, Hand PE, Micheal DC, Falcon LM, Yell AD, editors. Coal preparation in South Africa. 4th ed. Pietermaritzburg: The South African Coal Processing Society; 2002.
6. Sahoo R. Degradation characteristics of steel making materials during handling. Powder Technol. 2007;176(2):77–87. http://dx.doi.org/10.1016/j.powtec.2007.02.013
7. Tavares LM, De Carvalho RM. Modeling ore degradation during handling using continuum damage mechanics. Int J Miner Process. 2011;101(1):21–27. http://dx.doi.org/10.1016/j.minpro.2010.07.008
8. Le Roux M. The effect of thermal drying on the mechanical strength of South African coals. J S Afr I Min Metall. 2008;108:783–787.
9. Le Roux M, Campbell QP. An investigation into an improved method of fine coal dewatering. Minerals Eng. 2003;16(10):999–1003. http://dx.doi.org/10.1016/j.mineng.2003.08.004
10. Le Roux M, Campbell QP, Watermeyer MS, De Oliveira S. The optimization of an improved method of fine coal dewatering. Minerals Eng. 2005;18(9):931–934. http://dx.doi.org/10.1016/j.mineng.2005.01.033
11. Oberholzer V, Van der Walt J. Investigation of factors influencing the attrition breakage of coal. J S Afr I Min Metall. 2009;109(4):211–216.
12. Broadbent SR, Callcott TG. Coal Breakage Processes: III. The Analysis of a Coal Transport System. J I Fuel. 1957;30:13–25.
13. Sahoo R, Roach D. Quantification of the lump coal breakage during handling operation at the gladstone port. Chem Eng Process. 2005;44(7):797–804. http://dx.doi.org/10.1016/j.cep.2004.09.004
14. Paprika MJ, Komatina MS, Dakic DV, Nemoda SD. Prediction of coal primary fragmentation and char particle size distribution in fluidized bed. Energ Fuel. 2013;27(9):5488–5494. http://dx.doi.org/10.1021/ef400875q
15. Senneca O, Urciuolo M, Chirone R. A semidetailed model of primary fragmentation of coal. Fuel. 2013;104:253–261. http://dx.doi.org/10.1016/j.fuel.2012.09.026
16. Van Dyk JC. Development of an alternative laboratory method to determine thermal fragmentation of coal sources during pyrolysis in the gasification process. Fuel. 2001;80(2):245–249. http://dx.doi.org/10.1016/S0016-2361(00)00089-2

17. Zhang H, Cen K, Yan J, Ni M. The fragmentation of coal particles during the coal combustion in a fluidized bed. Fuel. 2002;81(14):1835–1840. http://dx.doi.org/10.1016/S0016-2361(02)00111-4

18. Bunt JR, Wagner NJ, Waanders FB. Carbon particle type characterization of the carbon behaviour impacting on a commercial-scale Sasol-Lurgi FBDB gasifier. Fuel. 2009;88(5):771–779. http://dx.doi.org/10.1016/j.fuel.2008.11.021

19. Senneca O, Russo S, Chirone R. Primary fragmentation of coal particles at high heating rate. Chem Eng Trans. 2009;18:569–574. http://dx.doi.org/10.3303/CET0918092

20. Powell MS, Morrison RD. The future of comminution modelling. Int J Miner Process. 2007;84(1):228–239. http://dx.doi.org/10.1016/j.minpro.2006.08.003

21. Han T, Kalman H, Levy A. Theoretical and experimental study of multi-compression particle breakage. Adv Powder Technol. 2003;14(5):605–620. http://dx.doi.org/10.1163/156855203322448372

22. Chandramohan R, Holtham P, Powell M. The influence of particle shape in rock fracture. Paper presented at: XXV International Mineral Processing Congress; 2010 Sept 6–10; Brisbane, Australia.

23. Tavares LM, King RP. Single-particle fracture under impact loading. Int J Miner Process. 1998;54(1):1–28. http://dx.doi.org/10.1016/S0301-7516(98)00005-2

24. Sahoo R. Review: An investigation of single particle breakage tests for coal handling system of the gladstone port. Powder Technol. 2006;161(2):158–167. http://dx.doi.org/10.1016/j.powtec.2005.09.001

25. Esterle JS, Kolatschek Y, O'Brien G. Relationship between in situ coal stratigraphy and particle size and composition after breakage in bituminous coals. Int J Coal Geol. 2002;49(2):195–214. http://dx.doi.org/10.1016/S0166-5162(01)00077-5

26. Shi F, Kojovic T. Validation of a model for impact breakage incorporating particle size effect. Int J Miner Process. 2007;82(3):156–163. http://dx.doi.org/10.1016/j.minpro.2006.09.006

27. Poulsen BA, Adhikary DP. A numerical study of the scale effect in coal strength. Int J Rock Mech Min Sci. 2013;63:62–71. http://dx.doi.org/10.1016/j.ijrmms.2013.06.006

28. Dacombe P, Pourkashanian M, Williams A, Yap L. Combustion-induced fragmentation behavior of isolated coal particles. Fuel. 1999;78(15):1847–1857. http://dx.doi.org/10.1016/S0016-2361(99)00076-9

29. Tavares LM, Das Neves PB. Microstructure of quarry rocks and relationships to particle breakage and crushing. Int J Miner Process. 2008;87(1–2):28–41. http://dx.doi.org/10.1016/j.minpro.2008.01.007

30. Mazumder S, Wolf KAA, Elewaut K, Ephraim R. Application of X-ray computed tomography for analyzing cleat spacing and cleat aperture in coal samples. Int J Coal Geol. 2006;68(3–4):205–222. http://dx.doi.org/10.1016/j.coal.2006.02.005

31. Van Geet M, Swennen R. Quantitative 3D-fracture analysis by means of microfocus X-ray computer tomography: An example from coal. Geophys Res Lett. 2001;28(17):3333–3336. http://dx.doi.org/10.1029/2001GL013247

32. Falcon RMS, Snyman CP. An introduction to coal petrography: Atlas of petrographic constituents in the bituminous coals of southern Africa. Johannesburg: The Geological Society of South Africa; 1986.

33. Van Geet M, Swennen R, Wevers M. Towards 3-D petrography: Application of microfocus computer tomography in geological science. Comput Geosci. 2001;27(9):1091–1099. http://dx.doi.org/10.1016/S0098-3004(00)00154-0

34. Laubach SE, Marret RA, Olson JE, Scott AR. Characteristics and origins of coal cleat: A review. Int J Coal Geol. 1998;35:175–207. http://dx.doi.org/10.1016/S0166-5162(97)00012-8

35. Ward CR. Analysis and significance of mineral matter in coal seams. Int J Coal Geol; 2002;50(1):135–168. http://dx.doi.org/10.1016/S0166-5162(02)00117-9

36. Ketcham RA, Carlson WD. Acquisition, optimization and interpretation of X-ray computed tomographic imagery: Applications to the geosciences. Comput Geosci. 2001;27(4):381–400. http://dx.doi.org/10.1016/S0098-3004(00)00116-3

37. Mees F, Swennen R, Van Geet M, Jacobs P. Applications of X-ray computed tomography in the geosciences. In: Mees F, Swennen R, Van Geet M, Jacobs P, editors. Applications of X-ray computed tomography in the geosciences. London: Geological Society of London; 2003. p. 1–6. http://dx.doi.org/10.1144/gsl.sp.2003.215.01.01

38. Duliu OG. Computer axial tomography in geosciences: An overview. Earth-Sci Rev. 1999;48(4):265–281. http://dx.doi.org/10.1016/S0012-8252(99)00056-2

39. Cnudde V, Boone MN. High-resolution X-ray computed tomography in geosciences: A review of the current technology and applications. Earth-Sci Rev. 2013;123:1–17. http://dx.doi.org/10.1016/j.earscirev.2013.04.003

40. Hoffman JW and De Beer FC. Characteristics of the Micro-Focus X-Ray Tomography Facility (MIXRAD) at Necsa in South Africa. Paper presented at: 18th World Conference on Nondestructive Testing; 2012 Apr 16–20; Durban, South Africa.

41. Ketcham RA, Slottke DT, Sharp JM. Three-dimensional measurement of fractures in heterogeneous materials using high-resolution X-ray computed tomography. Geosphere. 2010;6(5):499–514. http://dx.doi.org/10.1130/GES00552.1

42. Keller A. High resolution, non-destructive measurement and characterization of fracture apertures. Int J Rock Mech Min Sci. 1998;35(8):1037–1050. http://dx.doi.org/10.1016/S0148-9062(98)00164-8

43. Cnudde V, Masschaele B, Dierick M, Vlassenbroeck J, Hoorebeke LV, Jacobs P. Recent progress in X-ray CT as a geosciences tool. Appl Geochem. 2006;21(5):826–832. http://dx.doi.org/10.1016/j.apgeochem.2006.02.010

44. Krimmel S, Stephan J, Baumann J. 3D computed tomography using a microfocus X-ray source: Analysis of artifact formation in the reconstructed images using simulated as well as experimental projection data. Nucl Instrum Meth A. 2005;542(1–3):399–407. http://dx.doi.org/10.1016/j.nima.2005.01.171

45. Simons FJ, Verhelst F, Swennen R. Quantitative characterization of coal by means of microfocal X-ray computed microtomography (CMT) and color image analysis (CIA). Int J Coal Geol 1997;34(1):69–88. http://dx.doi.org/10.1016/S0166-5162(97)00011-6

46. Van Geet M, Swennen R, David P. Quantitative coal characterisation by means of microfocus X-ray computer tomography, colour image analysis and back-scattered scanning electron microscopy. Int J Coal Geol. 2001;46(1):11–25. http://dx.doi.org/10.1016/S0166-5162(01)00006-4

47. Dhillon RK, Singh P, Gupta SK, Singh S, Kumar R. Study of high energy (MeV) N6+ ion and gamma radiation induced modifications in low density polyethylene (LDPE) polymer. Nucl Instrum Meth B. 2013;301:12–16. http://dx.doi.org/10.1016/j.nimb.2013.02.014

48. Naudé G, Hoffman J, Theron SJ, Coetzer G. The use of X-ray computed tomography in the characterisation of coal and associated char reductants. Minerals Eng. 2013;52:143–154. http://dx.doi.org/10.1016/j.mineng.2013.05.012

49. Van Geet M, David P, Swennen R. Three dimensional coal characterisation (maceral, mineral and cleats) by means of X-ray microfocus computer tomography (μCT). Proceedings of the European Coal Conference IV; 2000 Sept 26–28; Poland, Uströn. Warsaw: Polish Geological Institute; 2002. p. 263–270.

50. Mathews JP, Pone JDN, Mitchell GD, Halleck P. High-resolution X-ray computed tomography observations of the thermal drying of lump-sized subbituminous coal. Fuel Process Technol. 2011;92(1):58–64. http://dx.doi.org/10.1016/j.fuproc.2010.08.020